Short Communication

Improved Electrochemical Cyclic Performances of Spinel LiMn$_2$O$_4$ by Coating with Lanthanum Phosphate

Yiqi Cui [1,2], Chengyi Zhu[3,*], Rui Huang[4], Jiaming Liu[5], Yannan Zhang[3,*]

[1] Faculty of Land Resource Engineering, Kunming University of Science and Technology, Kunming 650093, China
[2] Yunnan Province Engineering Research Center for Reutilization of Metal Tailings Resources, Kunming 650093, China
[3] Faculty of Metallurgical and Energy Engineering, Kunming University of Science and Technology, Kunming 650093, China
[4] Sino-Pipeline International Company Limited, Beijing 100000, China
[5] School of Metallurgy Engineering, Jiangxi University of Science and Technology, Ganzhou 341000, China
[*]E-mail: zhuchengyi1994@163.com (Chengyi Zhu), zyn_legolas@163.com (Yannan Zhang)

LiMn$_2$O$_4$ is regarded as a promising positive material candidate for contemporary lithium-ion batteries (LIBs) in terms of high safety, low cost, and environmental benignity. However, the spinel LiMn$_2$O$_4$ electrodes suffer from rapid capacity fades during lithiation and delithiation at high temperatures. Herein, we describe a simple sol-gel reaction method to modify the surface of LiMn$_2$O$_4$ materials and fill the gaps between particles by LaPO$_4$ to improve its electrochemical performance and utilization in the room and high temperature. As a result, the as-prepared LiMn$_2$O$_4$@ LaPO$_4$ electrode delivers excellent reversible capacity retention of 81.3% after 200 cycles at 1 C rate and exhibits a remarkable capacity of 74.9 mAh g^{-1} at 10 C rate. Moreover, Mn dissolution measurement reveals that LaPO$_4$ coating can effectively reduce the manganese dissolution in electrolytes at high temperatures. This general surface-modification strategy will have implications in practical applications for long-life lithium-ion batteries.

1. INTRODUCTION

With the constantly rapid development of technology, lithium-ion batteries (LIBs) have received tremendous attention as the preferred power source for portable devices and electric vehicles [1-3]. In particular, spinel LiMn$_2$O$_4$ has been recognized as a promising positive material candidate for

contemporary LIBs owing to its high operation potential, high safety, nontoxicity, and abundant manganese resource [4]. However, the large-scale commercial application of $LiMn_2O_4$ based LIBs are limited by rapid capacity fading during lithiation and delithiation, especially under high temperature. The performance deterioration of $LiMn_2O_4$ electrode mainly origins from the fast dissolution of manganese in the organic electrolyte and its low electrical conductivity [5-7]. To resolve the aforementioned issue for achieving long-term cyclic stability, Many researcher groups have made great efforts to enhance the cyclic stability of $LiMn_2O_4$ at both room and high temperatures. Surface chemistry is of great importance to the cyclic stability of spinel $LiMn_2O_4$. The coating materials such as (Al_2O_3 [8], ZnO [9], AlF_3 [10], TiO_2 [11], ZrO_2 [12],V_2O_5 [13] have been reported to restrain capacity fading, showing the effectiveness of surface modification on spinel $LiMn_2O_4$ electrodes. Among the numerous supporting materials, $LaPO_4$ has been advanced to be a novel positive electrode candidate for LIBs because it has exhibited favorable resistances to both oxidation and acid corrosion at high temperatures, it can be used as an excellent lithium ion-conducting medium as well [14]. Therefore, $LaPO_4$ is considered to be an effective coating mater to enhance both cycling life and rate capability. In this report, we have introduced a facile sol-gel combined solid-state calcination method to get high-density $LaPO_4$ coated $LiMn_2O_4$ nano-particles. The as-prepared $LiMn_2O_4$@ $LaPO_4$ electrode exhibits excellent cycling performance and remarkable rate ability. Furthermore, the effects of $LaPO_4$ coating on the Mn dissolution of the modified sample at room and high temperatures are also investigated

2. EXPERIMENTAL METHODS

2.1 Synthesis of spinel $LiMn_2O_4$ nanoparticles

$LiMn_2O_4$ nanorods were prepared via a solid-state reaction route. $LiOH \cdot H_2O$ (Shanghai Aladdin Reagent) and β-MnO_2 (Hunan Qingchong Co. Ltd) were fully dispersed by deionized water with the mole ratio of Li:Mn = 1.05:2, after strong mechanical stirring for 3 h. Subsequently, the mixture was subjected to evaporating at 100°C for 10 h in a vacuum oven. Finally, the spinel $LiMn_2O_4$ particles were obtained after calcining at 800°C for 8 hours under air flow, which were labeled as LMO.

2.2 Synthesis of $LaPO_4$ coated $LiMn_2O_4$ products

$LaPO_4$ coated spinel $LiMn_2O_4$ positive materials were synthesized by a modified sol-gel method to control the condensation of lanthanum nitrate hexa hydrate (Aladdin Reagent, 99.9%) and phosphoric acid. At first, $LaPO_4$ solution was synthesized by using a certain amount of phosphoric acid and lanthanum nitrate hexa hydrate dispersed in distilled water. The as-prepared solution contains 0.6 g $LaPO_4$. Then, 5 g of the $LiMn_2O_4$ powder was added in 150 mL absolute ethanol with 3 h continuous stirring. After that, the as-prepared $LaPO_4$ solution was slowly added drop wise to the dispersed $LiMn_2O_4$ mixture. The mixture was stirred well, heated to 70°C and held for 8 h until the moisture was evaporated to desiccation. Subsequently, the resultant products were washed three times with deionized water and then dried in a vacuum oven at 100°C for 12 h. Finally, the dried products were heat-treated at 700°C for 8 h to yield $LaPO_4$ coated $LiMn_2O_4$ nanoparticles, which were labeled as LMO-LP.

2.3 Material characterization

The crystalline structures of the obtained LMO and LMO-LP nanoparticles were tested on X-ray diffraction (XRD, D/MAX-2500 X) using Cu Kα radiation (λ = 1.54056 Å) at 40 kV and 200 mA. The samples were scanned from 10° to 70° by a step-scan mode with a step width of 2° and a step time of 2 seconds. The morphology and element distribution of as prepared two samples were characterized through a field emission scanning electron microscopy (FESEM, Zeiss Supra 55VP, Germany) with energy dispersive spectrometer (EDS, PHI5000 Versa probe-II, USA). The Mn dissolution of as-prepared two samples was carried out by the inductively coupled plasma (ICP, THERMO-6000, USA).

The electrochemical performance measurements were conducted in CR2025 coin half-cells. The coin cell preparation and detailed electrochemical analysis procedures were following our previous reports [15]. Cells were cycled on a battery test system (BTS, LAND CT-3008, China) in a voltage window of 3.0 V and 4.3V (vs. Li$^+$/Li) at 25°C and 55°C, respectively. The rate performance was implemented under different current densities from 0.1~10 C with a voltage range of 3.0~4.3 V. The electrochemical impedance spectroscopy (EIS) was carried out through a CHI 660D electrochemical workstation (CHI 660D, China) in the frequency range from 100 kHz to 0.01 Hz with an amplitude of 5 mV.

3. RESULTS AND DISCUSSION

The elemental composition and crystallinity of LMO and LMO-LP are analyzed by X-ray diffraction. As shown in Figure 2, Both of the as-prepared two samples SHC shows the strong peaks within the 2θ range of 10-70°, all peaks can be well indexed to spinel structure of LiMn$_2$O$_4$ (JCPDS card No. 35-0782), and no obvious impurity peaks of crystalline lanthanum phosphate are found, revealing that the lanthanum phosphate layer after the coating route is amorphous and does not affect the structure of spinel LiMn$_2$O$_4$. These results are in good agreement with the previous reports in the literature [16,17].
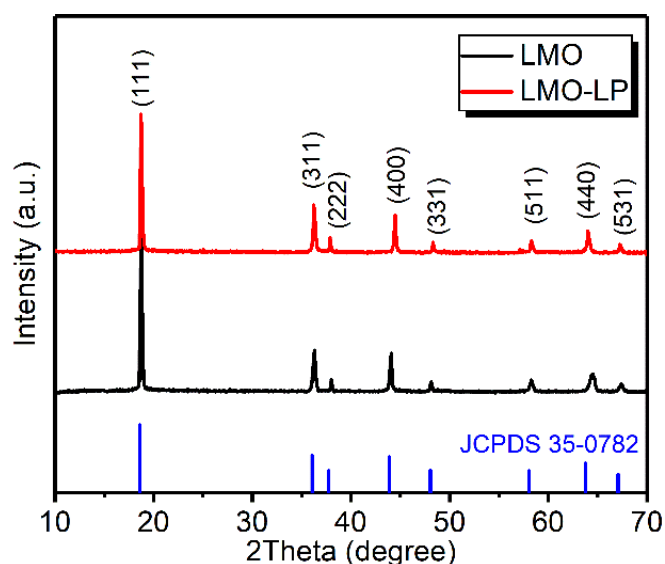

Figure 1. The XRD patterns of LMO and LMO-LP.

Figure. 2 displays the SEM image of LMO and LMO-LP nanoparticles. As can be seen from Fig. 2(a), the pristine $LiMn_2O_4$ particles have uniform particle size of 300~600 nm and well-defined morphology with smooth surface facets. Comparing with the pristine $LiMn_2O_4$ sample, Fig. 2(b) show that the surface of the LMO-LP powders changed noticeably after $LaPO_4$ coating, which displays slightly rougher surfaces, due to the presence of $LaPO_4$ layer. Smaller and uniform particles (around 10 nm) appear on the surface, and their density is very high on the LMO-LP sample. The occurrence indicates that the $LaPO_4$ layer on the pristine $LiMn_2O_4$ particles underwent some changes during the annealing process. Moreover, the energy dispersive spectroscopy (EDS) mappings of LMO-LP in Fig. 2(c-f) show that Mn, O, La, and P are homogeneously distributed on the surface of the pristine particles. Hence, we can conclude that $LaPO_4$ has been successfully introduced into the coating layers.
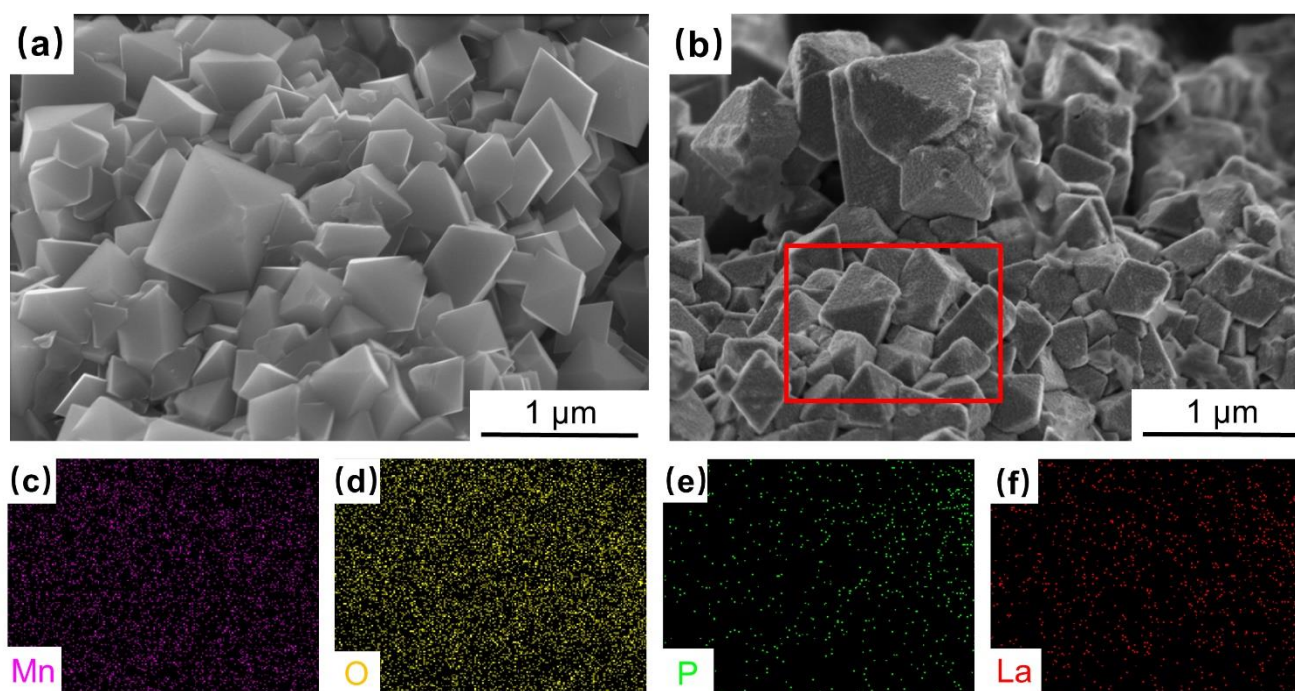

Figure 2. SEM imagines of LMO (a) and LMO-LP (b); EDS mapping images of LMO-LP (c-f).

The electrochemical tests are carried out to further investigate the effect of $LaPO_4$ coating layer on the electrochemical properties. Fig. 3a displays the 1st charge and discharge profiles of as-prepared samples at 0.1 C. It can be clearly seen that both of the two samples exhibit two distinct potential plateaus at approximately 4.10 V and 3.95 V, which are ascribed to the reversible transformation of $Li_{0.5}Mn_2O_4 \rightarrow Mn_2O_4$ and $LiMn_2O_4 \rightarrow Li_{0.5}Mn_2O_4$, respectively [18,19]. The initial discharge capacity of pristine $LiMn_2O_4$ is 132.3 mAh g^{-1}, while the LMO-LP electrode exhibit slightly lower discharge capacities of 129.5 mAh g^{-1}. This is because $LaPO_4$ is electrochemically inactive under 3.0~4.3 V *vs*. Li^+/Li, and the mass of active material per unit area on the electrode is reduced with the increase of the coating amounts, resulting in the decreasing of the initial capacity [20].

 Fig. 3c shows the rate performance of the two as-prepared samples at different rates from 0.1 to 10 C. Notably, comparing with LMO, LMO-LP delivers significantly improved discharge capacity with

the increase of rate, even at a high current density of 10 C, the sample of LMO-LP can still deliver a remarkable discharge capacity of 74.9 mAh g^{-1}, while the LMO exhibits the limited rate performance. Furthermore, when the rate returns to 1 C after discharging at a high rate (10 C), the LMO-LP electrode exhibits promising discharge capacity of 120.2 mAh g^{-1} and can retain 92.8% of their initial 0.1 C discharge capacity, which are significantly higher than that of uncoated one (113.9 mAh g^{-1}, 86.1%). These results clearly demonstrate that LMO-LP electrodes have promising structural stability and electrochemical reversibility.
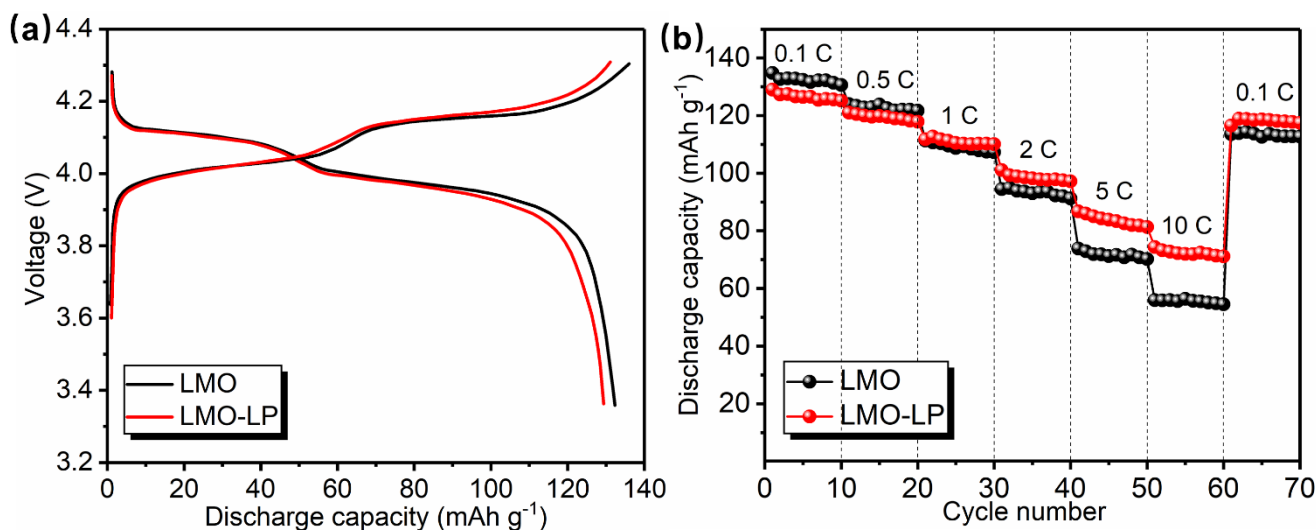

Figure 3. The initial charge/discharge curves of LMO and LMO-LP at 0.1 C rate (a); the rate performance of LMO and LMO-LP at different current density (b).

Fig. 5(a-b) shows the cycle performance of LMO and LMO-LP at 1 C rate under normal and high ambient temperature, respectively. As can be seen from Fig. 5(a), At room temperature (25°C), the LMO-LP delivers a higher discharge capacity retention (81.3 %) than the LMO materials (69.3 %) after 200 cycles even though both of the electrodes deliver almost the same initial discharge capacity. For a high temperature (55°C), the discharge capacity of the uncoated electrode decreases to 65.4 mAh g^{-1} from the initial 116.2 mAh g^{-1} after 200 cycles, delivering a capacity retention of only 56.3%. However, the LaPO$_4$-coated sample exhibits a significant improvement of capacity retention, the initial discharge capacity of the LMO-LP electrode is 118.3 mAh g^{-1}, which remains 85.3 mAh g^{-1} after 200 cycles. This result can be due to the following two factors: (1) the LaPO$_4$ coating can facilitate the formation of a more compaction conductive membrane, which provides a convenient path for Li$^+$ transport. (2) The outmost coating layer may suppress the generation of side reactions on the spinel LiMn$_2$O$_4$ surface and protect the active substance from being attacked by HF, thereby improving its rate performance and cycling life [21].
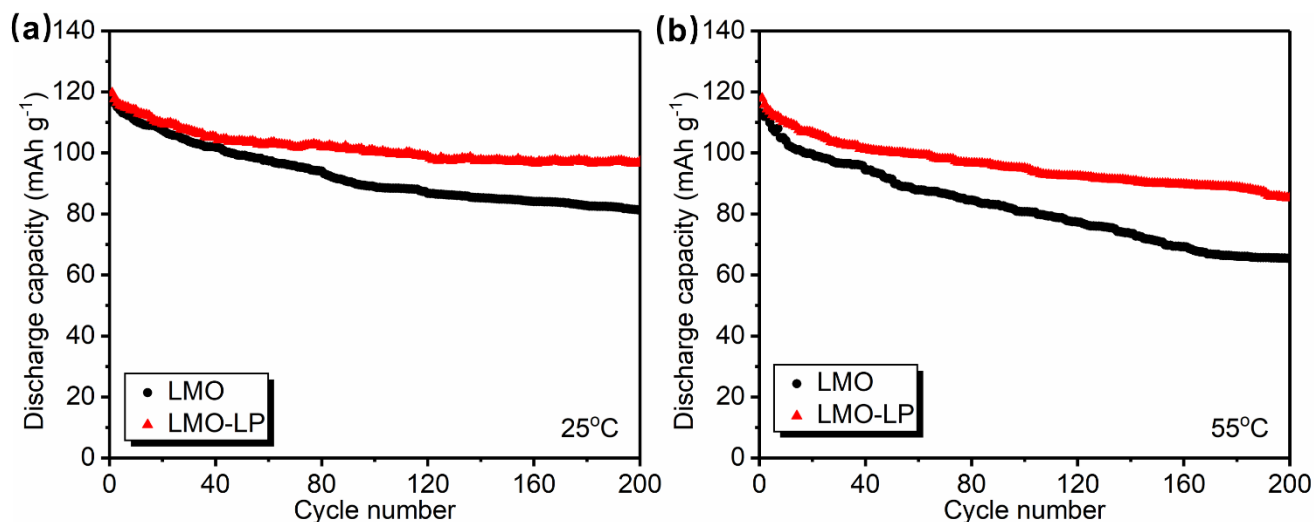
Figure 4. Cycling performances of LMO and LMO-LP samples at 1 C rate under 25°C (a) and 55°C (b).

To further verify above standpoint, the two electrodes stored in $LiPF_6$/EC: DEC (1:1) electrolyte at different temperatures are subjected to ICP-AES measurements for Mn dissolution. It can be clearly seen from Fig. 3 that the Mn dissolution in both of the samples is intensified over 7 days. Notably, the pristine LMO displays an obvious Mn dissolution as concentrations in the electrolyte is up to 36 and 75 ppm at 25°C and 55°C, respectively. However, the Mn concentrations of the LMO-LP electrodes in the same electrolyte are decreased to 12 and 18 ppm at 25°C and 55°C, respectively. These results clearly demonstrate that the $LaPO_4$ coating can significantly suppress the manganese dissolution in electrolytes and effectively restrain the generation of side reactions on the spinel electrode surface, which further confirms why LMO-LP electrodes have better reversibility than that of the uncoated pristine materials [22].
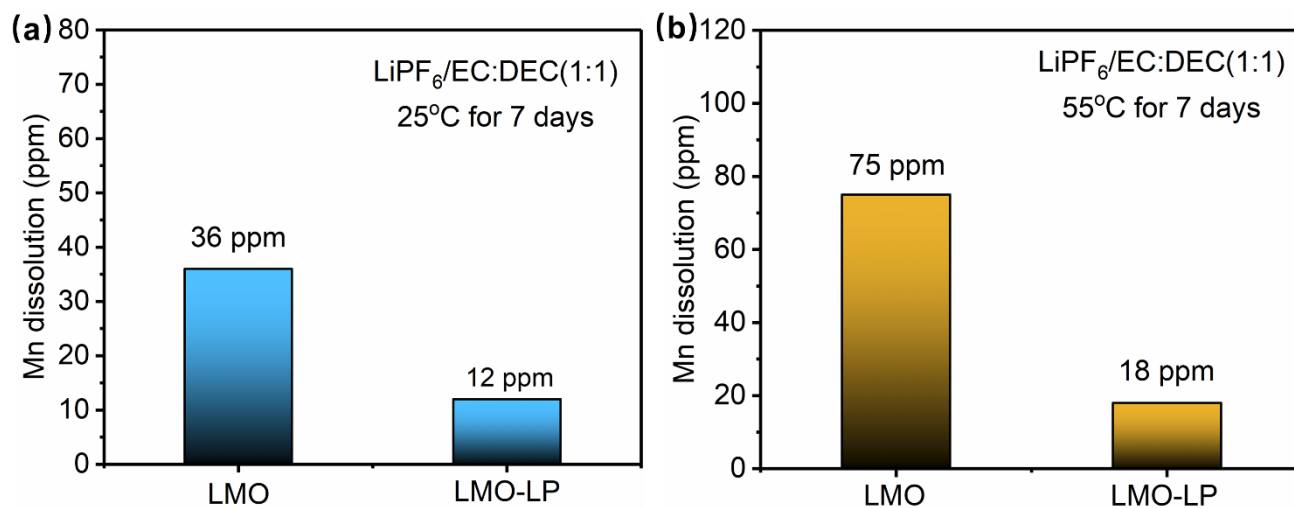

Figure 5. Concentration of Mn dissolved from LMO and LMO-LP samples stored in $LiPF_6$/EC: DEC (1:1) electrolyte at 25°C and 55°C for a week (c).

In addition, the lithium storage and cyclic properties of LiMn$_2$O$_4$@LaPO$_4$ are comparable to and even better than the previously state-of-the-art LiMn$_2$O$_4$ positive electrodes, as seen in Table 1.

Table 1. The comparison of LiMn$_2$O$_4$@LaPO$_4$ with the reported LiMn$_2$O$_4$ positive electrodes

LiMn$_2$O$_4$-based positive electrodes	Discharge capacity and capacity retention after several cycles at a certain rate
LiMn$_2$O$_4$@LaPO$_4$ (This work)	97.2 mAh g^{-1}, 81.3%, 200 cycles, 1 C
LiMn$_2$O$_4$ nanorods [26]	93.3 mAh g^{-1}, 79.6%, 200 cycles, 1 C
LiMn$_2$O$_4$@TiO$_2$ [11]	77.1 mAh g^{-1}, 62.0%, 250 cycles, 0.5 C
LiMn$_2$O$_4$@GO [27]	112.2 mAh g^{-1}, 87.1%, 100 cycles, 0.05 C
LiMn$_2$O$_4$@Co$_3$(PO$_4$)$_2$[28]	102.8 mAh g^{-1}, 87.0%, 100 cycles, 1 C
LiMn$_2$O$_4$@YPO$_4$ [29]	90 mAh g^{-1}, 84.1%, 100 cycles, 0.2 C

Electrochemical impedance spectroscopy (EIS) is further introduced to explore the electrochemical reaction kinetics of the as-prepared sample before and after 200 cycles, and the obtained Nyquist plots are shown in Figure 6. It can be seen that all plots are composed of a depressed semicircle in high-medium frequency region, which presents charge transfer resistance (Rct), and the oblique line in the low frequency assigned to lithium-ion diffusion processes in the electrode bulk [23-25]. It is obvious that both of the samples display a similar diameter of the semicircles before cycling.
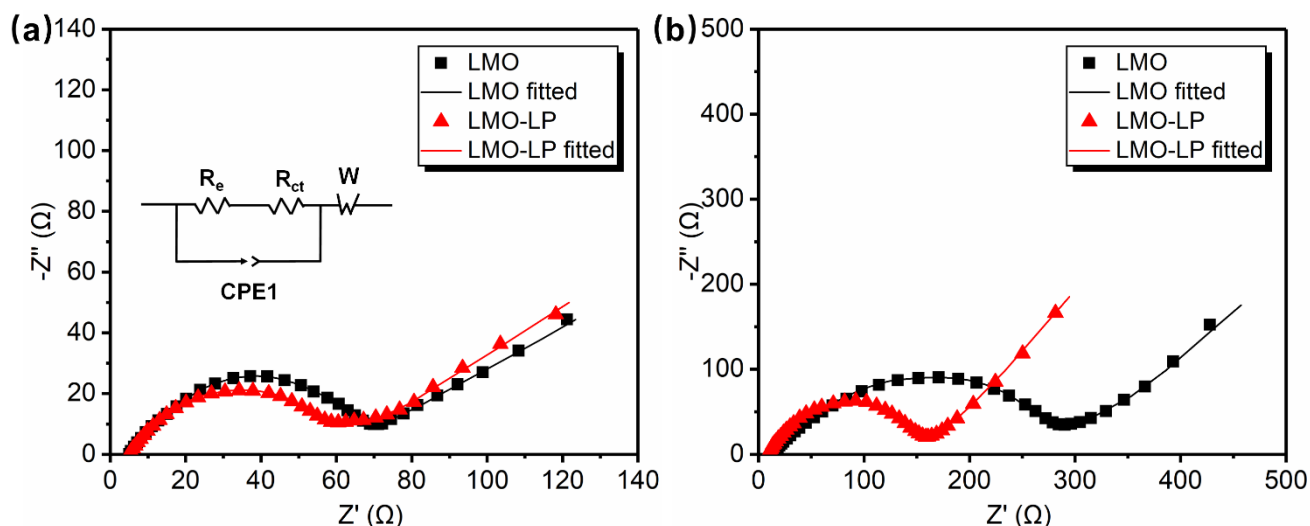

Figure 6. Impedance spectra (Nyquist plots) of LMO and LMO-LP tested before cycling (a) and after 200 cycles (b) at 1 C at room temperature.

However, when after 200 cycles, it can be clearly seen that the diameter of the semicircle of LMO electrodes is much larger than that of coated one and the solution resistance (R$_s$) of LMO is simulated as 7.9 Ω, which is lower than that of the pristine sample (13.7 Ω). The calculated charge-

transfer resistance of LMO-LP is 160 Ω, which is also lower than that of the uncoated electrode (295 Ω). The coated material has a smaller Rct, which also can restrain undesirable side reactions between the active material and electrolyte during the long cycling process. Thus, the introduction of $LaPO_4$ coating layer plays a key role in achieving enhanced Li^+ storage properties, the LMO-LP electrode displays promising electrochemical performance.

4. CONCLUSION

In summary, $LaPO_4$ coated $LiMn_2O_4$ positive materials (LMO-LP) were successfully synthesized through combined the sol-gel with the solid-state calcination methods. XRD and SEM analysis confirm that the as-prepared LMO-LP electrode displays the typical pristine structure combined with an uniform and continuous coating layer. The Mn dissolution of $LiMn_2O_4$ was effectively alleviated by this unique structure. Meanwhile, the impedance of the LMO-LP can be reduced by the $LaPO_4$ coating. Thus, the LMO-LP exhibits favorable cycle performance and outstanding rate performance (maintains a promising reversible discharge capacity of 85.3 mAh g^{-1} after 200 cycles at 55°C and delivers 74.9 mAh g^{-1} even at 10 C). This general surface modification strategy can also be further applied to develop other positive materials applied in energy and environmental science.

References

1. H. Guo, T. Li, W. Chen, L. Liu, X. Yang, Y. Wang and Y. Guo, *Nanoscale*, 6 (2014) 15168.
2. H. Liu, H. Guo, B. Liu, M. Liang, Z. Lv, K. R. Adair and X. Sun, *Adv. Fun. Mater.*, 28 (2018) 1707480.
3. J.M. Liu, R.X. Wang, X.C. Zhong, K. Yan, Y.H. Li and Z.F. Xu, *Int. J. Electrochem. Sci.*, 14 (2019) 1725.
4. Y. N. Zhang, Y. Y. Zhang, Y. J. Zhang, P. Dong, Q. Meng and M. L. Xu, *J. Alloy. Compd.*, 783 (2019) 357.
5. M. Okubo, Y. Mizuno, H. Yamada, J. Kim, E. Hosono, H. Zhou, T. Kudo, I. Honma, *ACS Nano*, 4 (2010) 741.
6. Z. Lu, X. Lu, J. Ding, T. Zhou, T. Ge, G. Yang, F. Yin and M. Wu, *Appl. Surf. Sci.*, 426 (2017) 19.
7. L. Su, P. Smith, P. Anand, and B. Jayan, *ACS Appl. Mater. Interfaces*, 10 (2018) 27063.
8. Y.N. Zhang, P. Dong, X.H. Yu, S.B. Xia, R.M. Yang, H.X. Liang, Z.Z. Shi, Y. Yao, X. Li and Y.J. Zhang. *Int. J. Electrochem. Sci.*, 12 (2017) 6853.
9. J. Tu, X.B. Zhao, J. Xie, G.S. Cao, D.G. Zhuang, T.J. Zhu, J.P. Tu, *J. Alloy. Compd.*, 432 (2007) 313.
10. A. Tron, Y.D. Park and J. Mun, *J. Power Sources*, 325 (2016) 360.
11. C. C. Zhang, X. Y. Liu, Q. L. Su, J. H. Wu, T. Huang and A. S. Yu, *ACS Sustainable Chem. Eng.*, 5 (2017) 640.
12. S. Hu, G. Cheng, M. Cheng, B. Hwang and R. Santhanam, *J. Power Sources*, 188 (2009) 564.
13. Q. Wu, K. Xue, X. H. Zhang, X. S. Xie, H. Q. Wang, J. J. Zhang and Q.Y. Li, *Ceram. Int.*, 45 (2019) 5072.

14. P. Mohan and G. Paruthimal Kalaignan, *Ceram. Int.*, 40 (2014) 1415.
15. Y.N. Zhang, P. Dong, M.Y. Zhang, X.L. Sun, X.H. Yu, J.J. Song, Q. Meng, X. Li and Y.J. Zhang, *J. Appl. Electrochem.*, 48 (2018) 135-145.
16. L. B. Ben, H. L. Yu, B. Chen, Y. Y. Chen, Y. Gong, X. N. Yang, L. Gu and X. J. Huang, *ACS Appl. Mater. Interfaces*, 9 (2017) 35463.
17. Y.N. Zhang, Y.J. Zhang, M.Y. Zhang, M.L. Xu, X. Li, X.H. Yu and P. Dong, *JOM*, 5 (2018) 1007.
18. L. Xiao, Y. L. Guo, D. Y. Qu, B. H. Deng, H. X. Liu and D. P. Tang, *J. Power Sources*, 225 (2013) 286.
19. C.Y. Zhu, J.X. Liu, X.H. Yu, Y.J. Zhang, P. Dong, X. Wang and Y.N. Zhang, *Ceram. Int.*, 45 (2019) 19351.
20. K.S. Fei, Q.H. Fei, F. Yao, L. Xi and W.Y. Gang, *Electrochim. Acta*, 144 (2014) 22.
21. Q. Liang, N. Cao, Z.H. Song, X.J. Gao, L.N. Hou, T.R. Guo and X, Qin, *Electrochim. Acta*, 251 (2017) 407.
22. K. Amine, J. Liu, S. Kang, I. Belharouak, Y. Hyung, D. Vissers and G. Henriksen, *J. Power Sources*, 129 (2004) 14.
23. G.D. Sheng andW. Ying, Ionics, 19 (2012) 1.
24. M. Wang, Y. Q. Gong, Y.J. Gu, Y.B. Chen, L. Chen and H. Shi, *Ceram. Int.*, 45 (2019) 3177.
25. F.X. Wu and G. Yushin, *Energy Environ Sci.*, 10 (2017) 435.
26. C.Y. Zhu, Y.N Zhang, X.H. Yu, P. Dong, J.G. Duan, J.M. Liu, J.X. Liu and Y.J. Zhang, *Chemsuschem*, 13 (2020) 803.
27. N. Kumar, J.R. Rodriguez, V.G. Pol, A. Sen, *Appl. Surf. Sci.,* 463 (2019) 132.
28. X.Y. Feng, J.X. Zhang, L.W. Yin, *Powder Technol*., 287:(2016) 77.
29. S. Zhao, Y. Bai, L. H. Ding, B. Wang and W. F. Zhang, *Solid State Ionics*, 247 (2013) 22.